Polymer Degradation and Stability 99 (2014) 223–232

Contents lists available at ScienceDirect

Polymer Degradation and Stability

journal homepage: www.elsevier.com/locate/polydegstab

Desorption electrospray ionisation mass spectrometry of stabilised polyesters reveals activation of hindered amine light stabilisers

Martin R.L. Paine [a], Ganna Gryn'ova [b], Michelle L. Coote [b], Philip J. Barker [c], Stephen J. Blanksby [a,*]

[a] ARC Centre of Excellence for Free Radical Chemistry and Biotechnology, School of Chemistry, University of Wollongong, Northfields Ave, Wollongong NSW 2522, Australia
[b] ARC Centre of Excellence for Free Radical Chemistry and Biotechnology, Research School of Chemistry, Australian National University, Canberra ACT 0200, Australia
[c] BlueScope Steel Research, PO Box 202, Port Kembla NSW 2505, Australia

ARTICLE INFO

Article history:
Received 11 September 2013
Received in revised form
14 October 2013
Accepted 31 October 2013
Available online 14 November 2013

Keywords:
Mass spectrometry
Polyester
Hindered amine light stabiliser
Mechanism

ABSTRACT

The use of hindered amine light stabilizers (HALS) to retard thermo- and photo-degradation of polymers has become increasingly common. Proposed mechanisms of polymer stabilisation involve significant changes to the HALS chemical structure; however, reports of the characterisation of these modified chemical species are limited. To better understand the fate of HALS and determine their *in situ* modifications, desorption electrospray ionisation mass spectrometry (DESI-MS) was employed to characterise ten commercially available HALS present in polyester-based coil coatings. TINUVIN® 770, 292, 144, 123, 152, and NOR371; HOSTAVIN® 3052, 3055, 3050, and 3058 were separately formulated with a pigmented, thermosetting polyester resin, cured on metal at 262 °C and analysed directly by DESI-MS. High-level *ab initio* molecular orbital theory calculations were also undertaken to aid the mechanistic interpretation of the results. For HALS containing *N*-substituted piperidines (*i.e.*, *N*–CH_3, *N*–$C(O)CH_3$, and *N*–OR) a secondary piperidine (*N*–H) analogue was detected in all cases. The formation of these intermediates can be explained either through hydrogen abstraction based mechanisms or direct *N*–OR homolysis with the former dominant under normal service temperatures (*ca.* 25–80 °C), and the latter potentially becoming competitive under the high temperatures associated with curing (*ca.* 230–260 °C).

1. Introduction

Many contemporary synthetic polymers require one or more chemical additives to enable them to carry out an intended function effectively. In the surface coatings sector, for example, the polymer provides the binder for a coating and the pigment for the aesthetic, but several types of functional additive are also required for a successful formulation. Thus, additives for rheology control, pigment dispersion, wetting, levelling *etc.* are commonly found in a wide range of coating types. Many of these additives have performed the role for which they were designed after the coating has been applied and dried (or cured). However, additives such as UV-absorbers and the so-called hindered amine light stabilisers (HALS) function during the service lifetime of the coating, and their role is to retard the degradation of the coating caused by the continuous barrage of environmental insults which can lead to compromised performance. HALS have been commonly employed in automotive, wood and plastic coatings for decades [1–6], and the last 10 years has seen an increase in their use in coil coatings. Coil coating is a large-scale process for continuous painting of steel strip at speeds of up to 200 m min^{-1}. The pre-painted steel strip thus produced is used in many different applications, the most severe of which is that employed in roofing, where the product needs to retain good appearance in service for 20 years or more. In turn, this places considerable emphasis on HALS to preserve the aesthetic and functional roles of the surface coating by protecting the polymer from degradation. Therefore, the optimisation of these compounds for such applications is of considerable interest; however, this first requires a thorough understanding of the chemistry associated with the protection of polymers by HALS. It is widely believed that HALS operate as chain-breaking antioxidants, undergoing oxidation of a heterocyclic amine to an aminoxyl radical, although the exact mechanisms by which this occurs is still the subject of investigation. It is this persistent aminoxyl radical that acts as a free radical

* Corresponding author. Tel.: +61 2 4221 5484; fax: +61 2 4221 4287.
E-mail address: blanksby@uow.edu.au (S.J. Blanksby).

0141-3910/$ – see front matter © 2013 Elsevier Ltd. All rights reserved.
http://dx.doi.org/10.1016/j.polymdegradstab.2013.10.026

scavenging intermediate and is thought to be involved in converting deleterious free radicals to less harmful even-electron species. As a result, regeneration of the aminoxyl radical occurs, theoretically allowing the process to repeat indefinitely [7–16]. However, empirical evidence suggests that the protective effects are finite and the use of HALS only delays the failure of polymers rather than denying it. Thus stabilisation *via* HALS must consist of a more complex mechanism.

Recently, Hodgson and Coote [17] deployed high-level quantum chemical calculations to compare the kinetics and thermodynamics of a dozen different reaction pathways comprising over 30 individual reactions. This allowed critical assessment of all the previously suggested mechanisms. Hodgson and Coote's analysis shows most of the mechanisms are kinetically and/or thermodynamically disfavoured with even the most favourable mechanism subject to a large activation barrier ($\sim$150 kJ mol^{-1}) for one of its key steps [17]. Furthermore, this mechanism does not account for previous experimental observations that suggest *in situ* conversion of an alkoxyamine functional group (*N*–OR) – analogous to an intermediate expected in an aminoxyl radical regenerative mechanism – to a secondary piperidine (*N*–H). This phenomenon was observed following high temperature curing of the polymer-based coating as well as subsequent exposure of the coating to accelerated weathering conditions [18]. Concordant results have also been reported in the literature for the decomposition of 2,2,6,6-tetramethylpiperidine-based HALS under thermo- and photo-oxidative conditions [19,20].

The inability to account for these observations by any of the commonly accepted mechanisms sparked a follow-up computational study by Coote and co-workers in which a new mechanism was proposed to explain the catalytic free radical scavenging by HALS in organic materials [21]. In this proposed cycle, an aminoxyl radical traps a carbon-centred substrate radical to form an alkoxyamine, and is then regenerated in a cascade of reactions triggered by hydrogen atom abstraction at the β-position of the alkoxyamine *via* another substrate-derived radical. The resulting species rapidly undergoes β-scission to form a ketone and an aminyl radical, and the aminyl radical can then either be oxidised back to the aminoxyl or abstract a hydrogen atom to form a secondary amine (see Scheme 1) [21]. This secondary amine can re-enter the catalytic cycle *via* hydrogen abstraction with any number of substrate-derived radicals, depending on the relative concentrations. In species that degrade *via* tertiary substrate-derived radicals, for which β-hydrogen abstraction is not possible, alternative catalytic cycles were proposed depending on whether direct *N*–OR homolysis was possible or not (see Scheme 1) [21]. These were shown to be much less energetically favourable, thus providing an explanation for the lower catalytic efficiency of HALS in such cases. The activation of the HALS was also studied, and shown to vary depending on whether the starting material was a secondary amine, the *N*-methyl derivative or an alkoxyamine (see Scheme 2) [21].

This recent computational study, supported by previous experimental observations suggests there may be other major repositories for HALS outside of the traditional regenerative cycles. Therefore, the aim of this work is to investigate the changing functionalisation of the piperidine nitrogen by characterising the structural changes occurring to a range of HALS compounds in polymer-based coatings. In this study, the focus is on the changes that occur specifically during curing under typical curing conditions and what impact they have on the chemical structure of the HALS. This in turn has implications for its activation (and hence protective action) under subsequent in-service conditions.

We have employed desorption electrospray ionisation mass spectrometry (DESI-MS) for the analysis of ten polyester-based coil coatings each containing a different commercially available HALS compound (Fig. 1). The compounds selected are structurally diverse providing the four most common piperidinyl moieties (*i.e.*, *N*–H, *N*–CH_3, *N*–C(O)CH_3, and *N*-OR). It is noted that basic HALS (N–H, N–CH_3; pK_a 7.5–9.7) are not typically used in acid-catalysed, cross-linked polyesters as they interfere with the curing process. They are included here however, to provide insight into the changes in functionality of HALS that are associated with curing conditions. HALS compounds retained within the coating after cure are detected *in situ*, characterised by tandem mass spectrometry and the results are rationalised with the aid of high-level electronic structure calculations.

2. Methods

2.1. Reagents

Methanol and formic acid were HPLC grade (Crown Scientific, Minto NSW, Australia). Chloroform and acetone were AR grade (Crown Scientific, Minto NSW, Australia). The hindered amine light stabilisers; bis(2,2,6,6-tetramethyl-4-piperidinyl) sebacate (TIN770), bis(1,2,2,6,6-pentamethyl-4-piperidinyl) sebacate (TIN292), bis(1,2,2,6,6-pentamethyl-4-piperidinyl)-((3,5-bis(1,1-dimethylethyl)-4-hydroxyphenyl)methyl)butylmalonate (TIN144), bis(1-octyloxy-2,2,6,6-tetramethyl-4-piperidinyl) sebacate (TIN123), 2,4-bis(*N*-butyl-*N*-(1-cyclohexyloxy-2,2,6,6-tetramethyl-4-piperidinyl)amino)-6-(2-hydroxyethylamine)-1,3,5-triazine (TIN152), and oligomers based on *N*-2-butyl-*N*-2-*N*-4-bis(2,2,6,6-tetramethyl-1-propoxy-4-piperidyl)-N-4-[5-(2,2,6,6-tetramethyl-1-propoxy-4-piperidyl)pentyl]-1,3,5-triazine-2,4-diamine (TIN NOR371) were supplied by Ciba Specialty Chemicals (Basel, Switzerland) now BASF (Ludwigshafen, Germany) and were used without purification. The hindered amine light stabilisers; β-alanine-*N*-(2,2,6,6-tetramethyl-4-piperidinyl)-dodecyl ester and β-alanine-*N*-(2,2,6,6-tetramethyl-4-piperidinyl)-tetradecyl ester (HOST3052), 2-dodecyl-*N*-(2,2,6,6-tetramethyl-4-piperidinyl) succinimide (HOST3055), 7-oxa-3,20-diazadispiro[5.1.11.2]heneicosane-20-propanoic acid-2,2,4,4-tetramethyl-21-oxo-dodecyl ester (HOST3050), and 2-dodecyl-*N*-(1-acetyl-2,2,6,6-tetramethyl-4-piperidinyl) succinimide (HOST3058) were supplied by Clariant (Huningue, France) and were used without purification.

2.2. Preparation of coated steel panels

The topcoat paint system employed in these studies was a solvent-borne, polyester topcoat paint incorporating a melamine-formaldehyde cross-linker, acid catalysed and formulated for coil paint-line application. This sample was formulated as a wet paint mixture and found to be 45% w/w resin solids by thermogravimetry (Perkin–Elmer TGA 7). The bulk paint sample was sub-sampled and weighed into small containers providing an identical matrix for comparative HALS analysis. The paints were formulated to give a final concentration of each HALS that resulted in a molar equivalent of an aminoxyl radical precursor (*N*-R) to that of TIN123 added at 2% w/w of total resin solids. The coated samples that were used in this project were laboratory prepared upon a pre-primed (commercial chromated epoxy primer) panels of a 0.6 mm thick GALVALUME®-type steel substrate. Wet paint was applied using a #28 wire-wound draw-down bar then cured for 55 s in a fan forced oven set at 262 °C. Under these conditions, 55 s equates to a peak metal temperature of 232 °C.

2.3. Desorption electrospray ionisation-mass spectrometry (DESI-MS)

Metal panels with a thermosetting polyester-based coating were cut into small sections (7 × 25 mm) using hydraulic shears

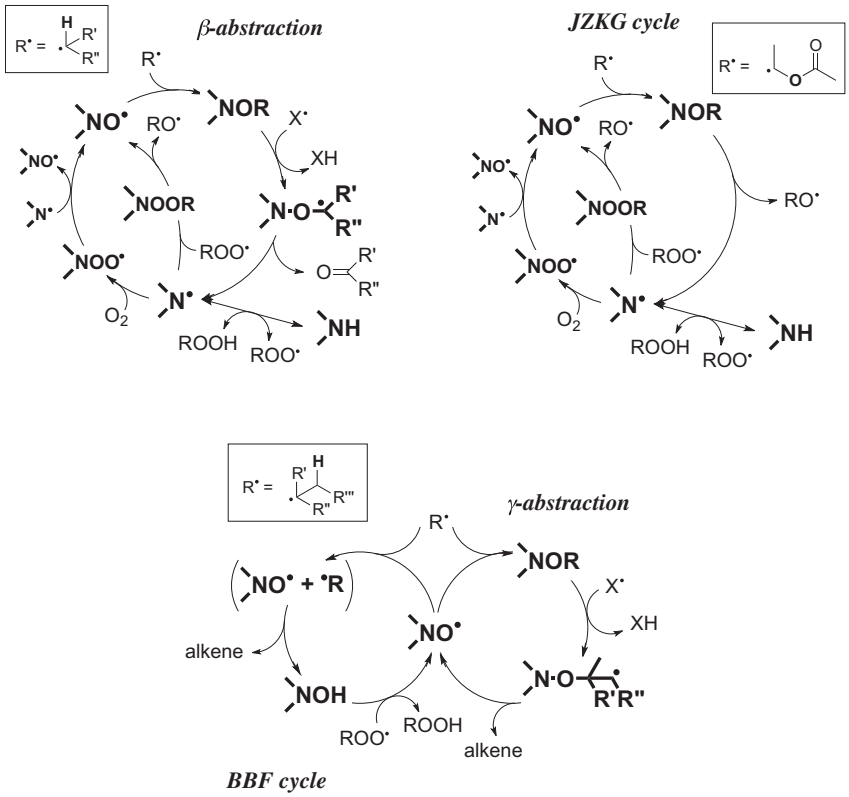

Scheme 1. Regeneration mechanisms for the catalytic protection of organic materials against autooxidation, as identified in Ref. [21]. The energetically preferred cycle for most combinations of aliphatic HALS is the β-abstraction. In cases where the degrading substrate radical does not contain an abstractable hydrogen, γ-abstraction or the JZKG cycle operate instead, the latter requiring preferred *N*–OR homolysis.

and affixed to a glass microscope slide. The samples were then placed in an enclosed atmosphere of acetone vapour for 5 min prior to DESI-MS analysis in order to swell the polymer, mobilising the HALS compounds to the surface of the substrate. Positive ion DESI-MS spectra were acquired using an Omni Spray® ion source (Prosolia Inc., Indianapolis, USA) coupled to a LTQ 2-dimensional (2-D) linear ion trap mass spectrometer (Thermo Fisher Scientific, San Jose, USA) with Xcalibur Tune Plus 2.0 software (Thermo Fisher Scientific, San Jose, USA) used for spectral acquisition. The DESI spray solvent, methanol acidified with 0.1% formic acid (v/v), was delivered at a flow rate of 10 μL min^{-1} with a 5 kV voltage applied to the spray emitter. MS instrument parameters were as follows: nebulising gas pressure, 80 psi; capillary voltage, 30 V; capillary temperature, 200 °C; sample holder velocity, 200 μm s^{-1}; ion

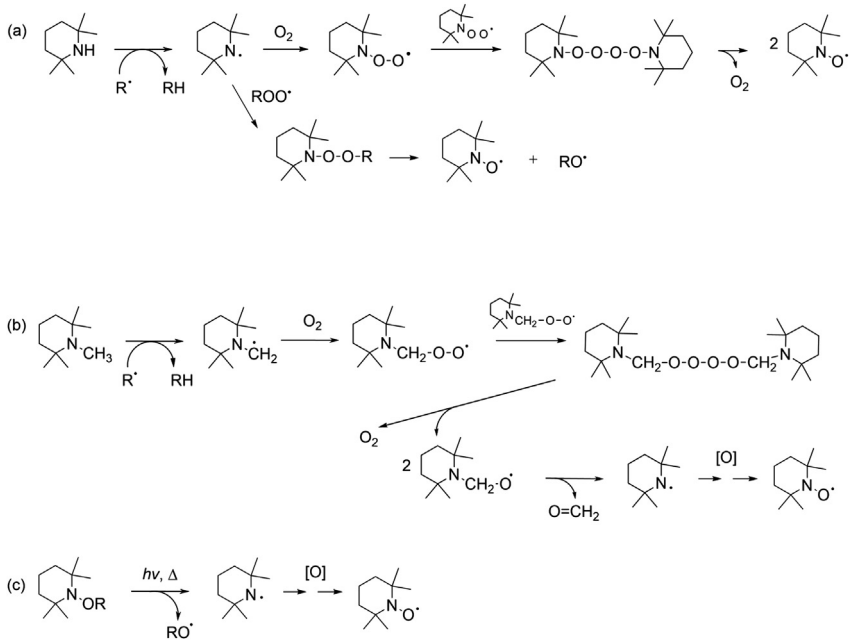

Scheme 2. HALS activation mechanisms for (a) secondary amines, (b) *N*-methyl amines, (c) alkoxyamines, as identified in Ref. [21].

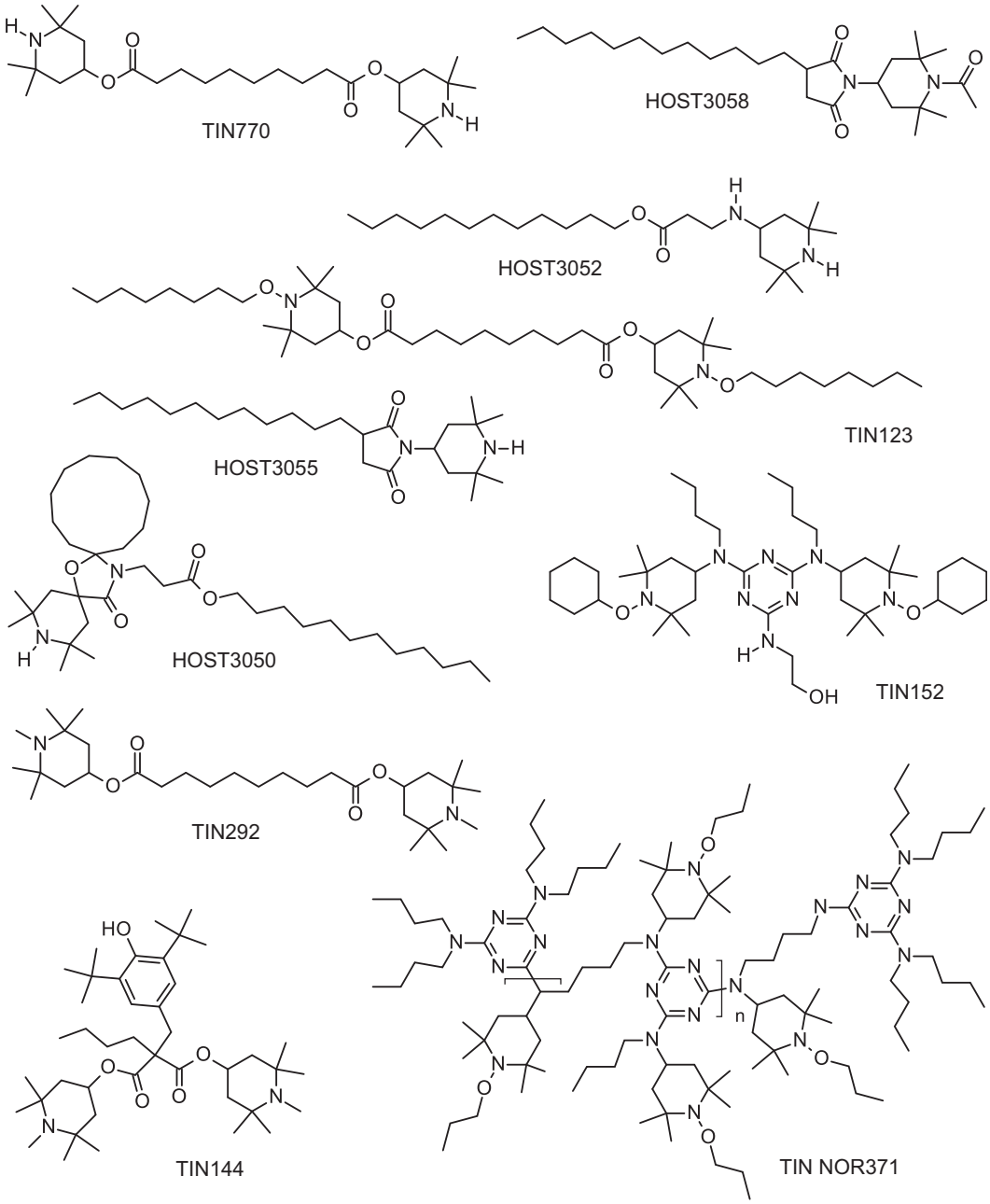

Fig. 1. The structures of the ten commercially available hindered amine light stabilisers (HALS) used in this study.

injection time, 30 ms; microscans, 2; with automatic gain control switched off. DESI-MS/MS spectra were acquired on the LTQ by subjecting trapped ions to pulsed-Q dissociation (PQD) [22], allowing detection of subsequent product ions below the conventional low mass cut-off of the ion-trap mass spectrometer. Typical experimental parameters for PQD were: isolation width, 1.5 Da; ion injection time, 50 ms; microscans, 2; collision energy 25–37 arbitrary units (See Table 1). Baseline subtraction was not used and mass spectra were averaged over a minimum of fifty scans. All mass spectra were normalised to the most abundant ion in the spectrum.

2.4. Computational procedures

Standard *ab initio* molecular orbital theory and density functional theory calculations were carried out using Gaussian 09 [23] and Molpro 2009.1 [24]. Calculations on radicals were performed with an unrestricted wave function except in cases designated with an "R" prefix where a restricted open-shell wave function was used. For all species, either full systematic conformational searches (at a resolution of 120°) or, for more complex systems, energy-directed tree searches [25] were carried out to ensure global, and not merely local minima were located. Geometries of all species were fully optimized at the B3-LYP/6-31G(d) level of theory and frequencies were also calculated at this level and scaled by recommended scale factors [26]. Accurate energies for all species were then calculated using double-layer ONIOM-type method. The core layer was calculated using the high-level composite *ab initio* G3(MP2)-RAD [26] method, whereas either R(O)MP2/6-311+G(3df,2p) (in homolysis studies) or M06-2X/6-311+G(3df,2p) (in activation mechanism modelling) method was applied to the full system. Entropies and thermal corrections at 25, 80 and 260 °C were calculated using standard textbook formulae [27] for the

Table 1
A summary of all DESI-MS/MS data acquired with a linear ion trap mass spectrometer following pulsed-Q dissociation (PQD) of selected precursor ions.

Formulated HALS	MS acquisition sequence	Product ions *m/z* (% abundance of base peak)
TIN770	MS^2 481.4 (PQD @ 27)	464.6 (4.94), 463.6 (1.27), 399.1 (3.44), 342.3 (100.00), 317.4 (1.17), 140.0 (15.15)
HOST3052	MS^2 425.4 (PQD @ 35)	351.9 (4.47), 324.3 (15.34), 312.3 (33.23), 140.0 (8.32)
	MS^2 397.4 (PQD @ 35)	388.5 (1.60), 284.2 (8.82), 140.1 (11.18)
HOST3055	MS^2 407.4 (PQD @ 35)	334.3 (100.00), 316.3 (4.27), 306.3 (8.23), 288.3 (1.72), 268.2 (4.95), 123.1 (9.29)
HOST3050	MS^2 633.6 (PQD @ 37)	542.5 (2.11), 450.5 (55.03), 434.4 (4.02), 394.3 (18.45), 328.3 (1.72), 180.0 (6.06), 166.1 (2.23), 138.0 (3.07)
	MS^2 605.6 (PQD @ 37)	514.5 (2.29), 422.5 (38.49), 406.4 (3.84), 366.3 (15.56), 328.3 (1.60), 180.0 (4.40), 166.1 (2.23), 138.1 (2.31)
TIN292	MS^2 509.5 (PQD @ 27)	491.4 (1.04), 478.4 (23.88), 356.3 (100.00), 154.1 (8.04)
	MS^2 495.5 (PQD @ 30)	477.4 (4.14), 464.4 (36.55), 463.2 (4.45), 437.1 (2.72), 435.3 (2.96), 363.3 (2.52), 356.3 (100.00), 342.3 (83.49), 154.0 (9.43)
TIN144	MS^2 685.5 (PQD @ 27)	654.5 (1.92), 532.4 (100.00), 466.1 (1.66), 429.1 (3.34), 341.0 (1.90), 219.1 (1.41)
	MS^2 671.5 (PQD @ 26)	532.4 (41.78), 518.3 (1.66)
HOST3058	MS^2 449.4 (PQD @ 35)	389.4 (1.88), 334.3 (37.89), 235.1 (11.74)
	MS^2 407.4 (PQD @ 35)	334.3 (100.00), 316.3 (3.98), 306.3 (8.17), 288.3 (1.26), 268.2 (4.14), 123.1 (7.95)
TIN123	MS^2 737.5 (PQD @ 25)	625.4 (12.97), 624.4 (6.51), 607.5 (3.13), 593.4 (3.54), 496.4 (100.00), 470.3 (6.04), 342.3 (2.04), 268.1 (1.45)
	MS^2 609.5 (PQD @ 25)	573.2 (5.21), 496.5 (18.80), 496.1 (11.82), 481.5 (3.03), 477.5 (10.11), 470.0 (6.29), 342.1 (30.45), 243.0 (6.50)
TIN152	MS^2 769.5 (PQD @ 30)	686.5 (14.05), 655.4 (6.60), 588.4 (74.51), 558.4 (29.25), 532.4 (100.00), 449.4 (3.46), 295.2 (6.43), 238.1 (10.04)
	MS^2 757.5 (PQD @ 28)	725.0 (2.26), 674.6 (5.90), 576.4 (22.02), 546.5 (4.79), 520.4 (37.55), 283.2 (3.72), 238.0 (1.97)
	MS^2 671.5 (PQD @ 30)	588.6 (1.43), 558.2 (2.12), 532.4 (100.00), 472.4 (1.44), 460.3 (3.86), 434.4 (19.90), 376.2 (1.24), 295.3 (5.22), 238.1 (2.70)
	MS^2 659.5 (PQD @ 26)	627.3 (7.52), 595.2 (9.54), 545.2 (7.81), 520.6 (31.01), 520.2 (18.62), 422.1 (11.83), 283.1 (10.17)
TIN NOR371	MS^2 1022.8 (PQD @ 35)	979.8 (78.26), 851.8 (12.59), 825.8 (100.00), 783.9 (1.56), 461.5 (1.63), 431.4 (1.49), 377.4 (1.88), 351.5 (1.26)
	MS^2 964.8 (PQD @ 35)	851.8 (7.30), 825.8 (100.00), 809.8 (1.35), 783.8 (12.22), 727.8 (2.09)

statistical thermodynamics of an ideal gas under the harmonic oscillator approximation in conjunction with the optimized geometries and scaled frequencies. Reaction Gibbs free energies were computed using Gibbs fundamental equation.

Free energies of solvation in toluene were calculated using the polarized continuum model PCM-UAKS [28]at the B3LYP/6-31G(d) level of theory. Free energies of each species in solution at 298.15 K were calculated as the sum of the corresponding gas-phase free energy and the obtained free energy of solvation. The phase change correction term ΔnRT(lnV) was added to the resulting free energies for each species.

3. Results and discussion

3.1. Positive ion DESI-MS of polyester-based coatings containing HALS

The ambient ionisation technique desorption electrospray ionisation-mass spectrometry (DESI-MS) has been employed herein for the detection of polymer additives in polyester-based coil coatings. To allow detection of HALS from thermoset coatings by DESI-MS a simple, non-destructive sample preparation method was developed by our research group that exposes the coatings to acetone vapour, partially swelling the coating and mobilising the additives to the surface for detection [18]. The samples were then positioned in a geometry that allowed a continuous flow of charged, pneumatically-assisted microdroplets from the DESI source to impact and wet the sample surface. HALS extracted into the localised solvent reservoir became entrained in secondary droplets released from the surface and upon drying resulted in gas phase ions that were detected by mass spectrometry. Positive ion DESI-MS spectra of polyester-based coatings containing each HALS separately, pre-treated in an acetone vapour bath for 5 min were recorded using a linear ion-trap mass spectrometer and are shown in Figs. 2–5. The spectra yield intense signals corresponding to the $[M + H]^+$ ion for each HALS resulting from protonation of the heterocyclic nitrogen or other basic sites present in the molecule. Structural confirmation of each HALS was achieved by tandem mass spectrometry – employing pulsed-Q dissociation (PQD) – of the $[M + H]^+$ ion with the resulting product ions reported in Table 1. PQD is a form of resonance excitation that allows ions of a selected *m/z* ratio to be isolated and activated to induce dissociation to product ions. The dissociation occurs as resonance activation of selected ions increases their kinetic energy, which is converted to internal energy through repeated collisions with buffer gas present in the ion trap. PQD differs from conventional collision-induced dissociation (CID) methods as it allows the observation of low *m/z* fragments that are usually excluded from CID spectra and also helps to access higher energy dissociation channels [22]. Fragmentation mechanisms and resulting product ions of HOST3055, TIN292, HOST3058, TIN123, and TIN152 have been characterised previously using electrospray ionisation tandem mass spectrometry (ESI-MS/MS) and the product ions reported here are congruent with that study [29]. For those HALS not previously characterised by comparable mass spectrometric techniques (TIN770, HOST3052, HOST3050, TIN144 and TIN NOR371), structures were inferred by a comparative analysis of their product ions arising from PQD (Table 1).

3.2. DESI-MS characterisation of TIN770, HOST3052, HOST3055, and HOST3050 (N–H)

Fig. 2(a–d) show DESI-MS spectra of four structurally diverse HALS (TIN770, HOST3052, HOST3055, and HOST3050) each containing 2,2,6,6-tetramethylpiperidine moieties unsubstituted at the nitrogen (*N*–H). All four spectra demonstrate an excellent signal-to-noise ratio for the peak corresponding to the $[M + H]^+$ ion except Fig. 2(b). The poor signal-to-noise ratio in this spectrum is due to HOST3052 being supplied as a mixture of up to five different structural analogues of the compound listed by the manufacturer (Fig. 2(b)). Spreading the peak intensity over four or more channels effectively reduces the signal-to-noise ratio and the contrast is easily observed by comparison with Fig. 2(c) as HOST3055 is present as only one ionisable species. The remaining unassigned peaks in Fig. 2(b) were confirmed to be chemical noise present in all ten DESI-MS spectra by comparison with the baseline of the spectrum in Fig. 2(c) at 20 times magnification, *i.e.*, the magnified baseline of Fig. 2(c) was observed to be identical to the baseline of Fig. 2(b).

3.3. Structural modifications to HALS in situ detected by DESI-MS

3.3.1. HALS TIN292 and TIN144 (N–CH_3)

Positive ion DESI-MS spectra after pre-treatment of two cured polyester-based coil coatings each containing structurally distinct

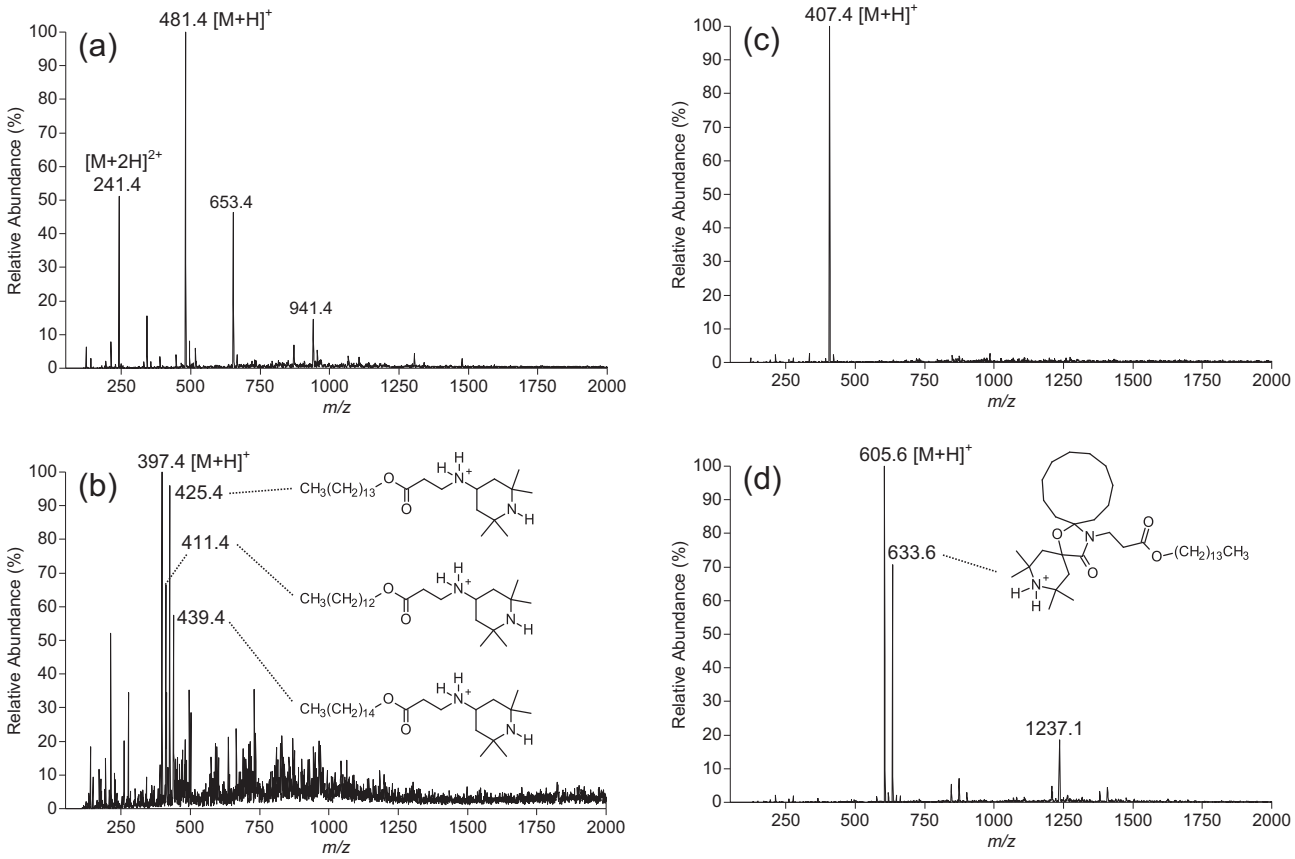

Fig. 2. (a–d). Positive ion DESI-MS spectra of TIN770, HOST3052, HOST3055, and HOST3050 detected within polyester-based coil coatings after pre-treatment with acetone vapour. Inset – Putative structures for oligomers and synthetic by-products of the precursor HALS compounds present.

compounds with two 1,2,2,6,6-pentamethylpiperidine moieties, TIN292 and TIN144, show peaks that are indicative of their respective $[M + H]^+$ ions (Fig. 3(a) *m/z* 509.5 and Fig. 3(b) *m/z* 685.5, respectively). These spectra also contain peaks at a mass-to-charge ratio 14 Da lower than the $[M + H]^+$ ions, *m/z* 495.5 and 671.5, respectively. Product ions arising from PQD activation of these species are listed in Table 1 and suggest a high degree of structural homology with their associated $[M + H]^+$ counterparts. The product ion spectra for both *m/z* 495.5 and 671.5 ions show a neutral loss of 153 Da from the precursor ion (Table 1; *m/z* 342.3 and 518.3, respectively); a loss also observed in the product ion spectra for TIN292 (*m/z* 356.3) and TIN144 (*m/z* 532.4). This neutral loss corresponds to the characteristic fragmentation product 1,2,2,6,6-pentamethyl-3*H*-pyridine that arises following elimination of the ester-bound substituent from the 4-position of the piperidine ring (Scheme 3) [29]. This unimolecular dissociation is driven by the non-bonding electron pairs on the ester moiety accepting a proton from the piperidine ring and forming a carbon–carbon double bond with loss of the substituent as a carboxylic acid [29–31]. Furthermore, the neutral loss of 139 Da is also observed from the *m/z* 495.5 and 671.5 precursor ions (Table 1; *m/z* 356.3 and 532.4, respectively) that, by the same rationale proposed for the above neutral loss, would correspond to the loss of 2,2,6,6-tetramethyl-1,3*H*-pyridine. This neutral loss is not observed in the product ion spectra for TIN292 and TIN144. The 14 Da mass difference and the PQD product ion spectra indicate that the ions at *m/z* 495.5 and 671.5 are protonated ions of TIN292 and TIN144 after conversion of one 1,2,2,6,6-pentamethylpiperidine moiety to a 2,2,6,6-tetramethylpiperidine (Fig. 3(a) and b; inset). The ions attributed to these compounds are unlikely to be in-source fragments as they are not present in the MS/MS spectra of the $[M + H]^+$ ions for TIN292 and TIN144 and are not present in the authentic HALS samples. Therefore, these ions are proposed to be evidence for *in situ* modifications facilitated by the curing conditions experienced by the polyester-based coil coating.

3.3.2. *HALS HOST3058 (N–C(O)CH$_3$)*

Positive ion DESI-MS spectrum of a cured polyester-based coil coating containing HOST3058 shows a peak that is indicative of the $[M + H]^+$ ion at *m/z* 449.4 (Fig. 4). However, this is one of two cases where the base peak in the spectrum is not at the *m/z* associated with the $[M + H]^+$ ion. In this spectrum, the peak at *m/z* 407.4, 42 Da lower than the molecular mass of HOST3058, is the base peak and is more than 10 times the relative abundance of the ionised HOST3058. This ion represents protonated 2-dodecyl-*N*-(2,2,6,6-tetramethyl-4-piperidinyl) succinimide (Fig. 4; inset) and is the synthetic precursor to HOST3058, being present at low levels in the authentic sample (data not shown). Product ions arising from PQD activation of *m/z* 407.4 (Fig. 4) are shown in Table 1 with the peak distribution and ion abundances almost identical to the PQD spectrum reported for HOST3055 (Table 1) thus confirming the identity as the secondary piperidine of HOST3058. This ion at *m/z* 407.4 is not present in the MS/MS spectrum for the ion at *m/z* 449.4 and therefore is not attributed to in-source fragmentation caused by instrument conditions, and is detected in higher abundances compared to that found in the authentic sample. This phenomenon may be attributed to either selective depletion of HOST3058 over the secondary piperidine during cure or, as is more likely, an increase in abundance of the secondary piperidine compared to HOST3058 resulting from *in situ* *N*-deacetylation of the 1-acetyl-

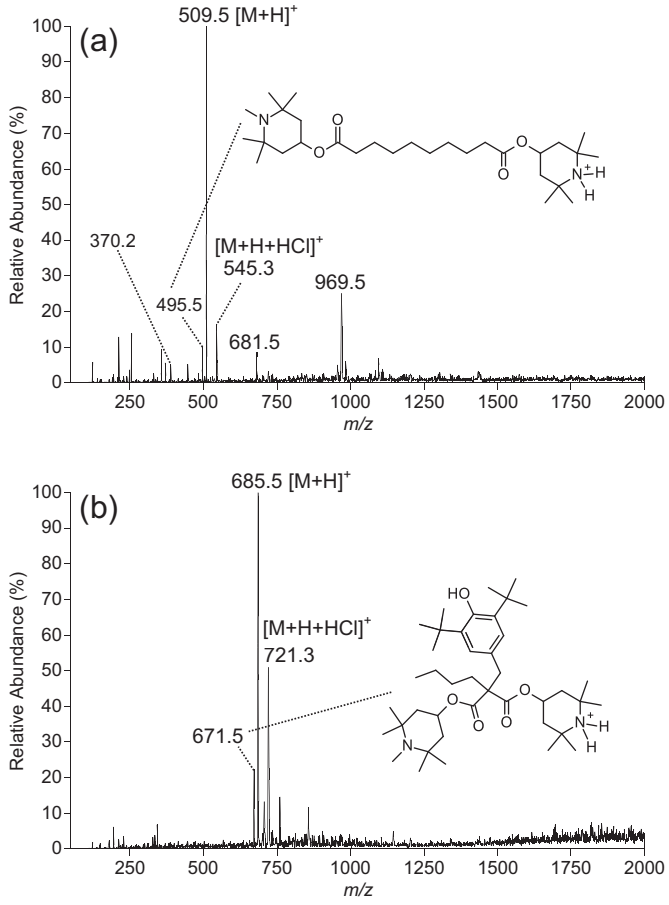

Fig. 3. (a and b) Positive ion DESI-MS spectra of TIN292 and TIN144 detected within polyester-based coil coatings after pre-treatment with acetone vapour. Inset – Putative structures for the *in situ* structural modifications to the precursor HALS compounds present. The ion at *m/z* 370 in the spectrum shown in (a) corresponds to a monofunctional derivative present in the TIN292 additive.

2,2,6,6-tetramethylpiperidine moiety to the 2,2,6,6-tetramethylpiperidine. This phenomenon has also been observed by ESI-MS and ESR analyses following solvent extraction of polyester-based coil coatings containing HOST3058 [29].

3.3.3. HALS TIN123, TIN152, and TIN NOR371 (N–OR)

Positive ion DESI-MS spectra of three polyester-based coil coatings each formulated with structurally distinct HALS compounds (TIN123, TIN152, and TIN NOR371) that contain two or more 2,2,6,6-tetramethylpiperidine moieties functionalised at the nitrogen with an alkoxyamine are shown in Fig. 5(a–c). TIN123 and TIN152 show peaks that are indicative of their respective $[M + H]^+$ ions at *m/z* 737.5 (Fig. 5(a)), and *m/z* 757.5 (Fig. 5(b)), respectively, with a monomeric fragment of TIN NOR371 (*m/z* 1022.8) detected in Fig. 5(c). Positive ion DESI-MS analysis of TIN123 present in polyester-based coil coatings has been well characterised previously [18] and structural modification of the alkoxyamine moiety to the secondary piperidine of TIN123 *in situ* (Fig. 5(a); inset).

The DESI-MS spectrum for TIN152 is another case where the base peak in the spectrum is not at the *m/z* associated with the $[M + H]^+$ ion. Fig. 5(b) shows the base peak at *m/z* 769.5, 12 Da higher than the protonated molecular mass of TIN152. The fragmentation pattern arising from the PQD of *m/z* 769.5 is shown in Table 1 and is similar to that of $[M + H]^+$ ion at *m/z* 757.5 suggesting a high degree of structural homology with TIN152. Tentative structural elucidation of the ion at *m/z* 769.5 using the PQD fragmentation pattern indicates that the aminoethanol group functionalised to the triazine is absent and an additional butyl group is present at this position (Fig. 5(b); inset). This is supported by the comparison between subsequent fragmentation of product ions generated by PQD of the ion at *m/z* 757.5 and 769.5 (Table 1) that show conservation of the 12 Da mass difference for the analogous ions all the way to the fragment corresponding to a substituted 1,3,5-triazine-2,4,6-triamine (*m/z* 283.2 and 295.2, respectively). Although this compound is not listed as a synthetic by-product by the supplier, analysis of an authentic sample of TIN152 under the same experimental conditions shows a very small relative abundance (<1%; data not shown) at the same *m/z*. The difference in relative abundances of these two components when detected in a cured thermosetting coating can be rationalised by the propensity for TIN152 to be co-condensed to the polymer backbone through condensation of the primary alcohol substituent to melamine and isocyanate cross-linkers and therefore not able to be liberated from the coating using standard DESI techniques.

Fig. 5(b) also exhibits peaks at *m/z* 659.5 and 671.5 corresponding to a mass loss of 98 Da from the $[M + H]^+$ ion of both TIN152 and the butylamino derivative (Fig. 5(b); inset). This mass difference equates to the substitution of one cyclohexyloxy group with hydrogen, consistent with the formation of a secondary piperidine for both TIN152 (Fig. 5(b); inset) and the butylamino derivative (Fig. 5(b); inset). These putative structures are supported by the detection of abundant product ions at *m/z* 520.2 and 532.4, respectively, corresponding to a 139 Da neutral loss from the precursor ions, which represents a loss of 2,2,6,6-tetramethyl-3*H*-pyridine and is indicative of the presence of a secondary piperidine moiety (*c.f.* Scheme 1). Again, these ions are not present in the analysis of authentic samples nor are they a result of in-source fragmentation caused by instrument conditions or listed as synthetic by-products listed by the supplier.

The positive ion DESI-MS spectrum of a cured polyester-based coil coating containing oligomeric TIN NOR371 after pre-treatment is shown in Fig. 5(c). The spectrum contains a dominant base peak at *m/z* 1022.8 that corresponds to the monomeric structure of the oligomer minus an *N*,*N*-dibutyl amino group (Fig. 1). The putative structure is supported by the MS/MS spectrum of ions at *m/z* 1022.8 (Table 1). PQD of the isolated ion yielded product ions at *m/z* 979.8 corresponding to the loss of a propyl radical from *N*O–C bond cleavage of the alkoxyamine and *m/z* 851 corresponding to the subsequent loss of an *N*,*N*-dibutylamino group. The major product ion at *m/z* 825 corresponds to the neutral loss of 197 Da (2,2,6,6-tetramethyl-1-propoxy-3*H*-pyridine) from the precursor resulting from elimination of 2,2,6,6-tetramethyl-1-propoxypiperidine following a highly characteristic fragmentation mechanism for HALS containing piperidine structures [29].

3.3.4. Computational investigations of mechanisms for N-modifications

The above experimental analysis of the all the major classes of HALS (*N*–*OR*, *N*–R and *N*–C(O)R) indicates *in situ* conversion of the substituted piperidine moiety to a secondary amine within pigmented polyester-based coil coatings during curing. Below we discuss the mechanistic implications of these results with the aid of computational chemistry.

3.3.5. N–OR HALS

The conversion of *N*–OR HALS to the corresponding secondary amine *N*–H under curing conditions (232 °C) echoes our earlier model spin-trapping ESR experiments for TIN123 at 80 °C (a typical service temperature), which detected the spin-trap adducts of an alkoxyl radical and α-phenyl-*N*-*tert*-butyl nitrone [18]. Collectively

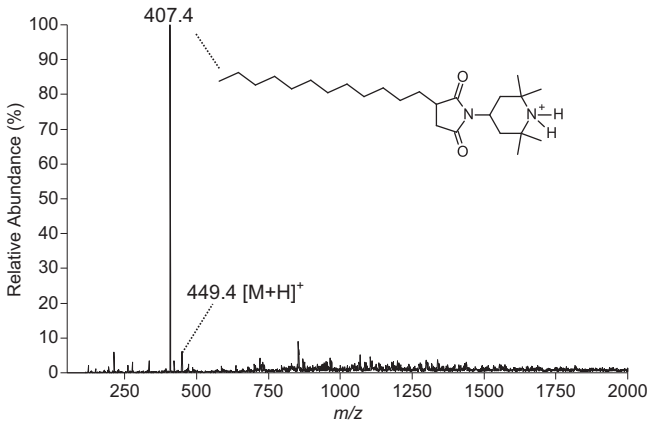

Fig. 4. Positive ion DESI-MS spectra of HOST3058 detected within polyester-based coil coatings after pre-treatment with acetone vapour. Inset – Putative structures for the *in-situ* structural modification to the precursor HALS compounds present.

these experimental observations are equally consistent with both the β-hydrogen abstraction based regeneration mechanism and the direct *N*–OR homolysis mechanisms of Scheme 1 [21]. Previous computational studies concluded that, even for a model polyester-derived radical for which *N*–OR and *NO*–R homolysis is equally likely, the β-hydrogen abstraction based regeneration mechanism was still more energetically favourable, even at typical service temperatures of 80 °C [21]. Moreover, other computational studies have shown that *N*–OR homolysis is uncompetitive with *NO*–R homolysis for most other leaving groups [17,32]. Nonetheless, in the present work we examine the *N*–OR and *NO*–R homolysis gas- and solution-phase enthalpies and Gibbs free energies (kJ mol^{-1}) for representative HALS (see Table 2). Table 2 shows results at 260 °C, which represents the upper end of typical curing temperatures; whilst the absolute Gibbs free energies are temperature dependent, the free energy differences themselves are relatively unaffected by temperature over the range studied (25–260 °C; see Table S1 of the Supporting Information).

Comparison of the calculated gas and solution-phase Gibbs free energies of *N*-OR and *NO*-R homolysis for the three alkoxyamine HALS investigated (Table 2) indicates that *NO*-R homolysis would be thermodynamically favoured in each case. However, the Gibbs free energy differences between *N*-OR and *NO*-R homolysis in these examples are small (*ca.* 10 kJ mol^{-1}), suggesting that *N*–OR homolysis could be occurring once every ten or so *NO*–R reactions at 260 °C (or once every 60 at 80 °C). Whilst neither *N*–OR nor *NO*–R is competitive with β-hydrogen abstraction pathway at room temperature or service temperatures such as 80 °C [21], homolysis *per se* becomes relatively more important at the high temperatures associated with curing (*e.g.*, 260 °C) due to its entropic favourability. Under those circumstances, it is conceivable that, for these simple alkyl leaving groups, *N*–OR homolysis may play a minor role. For example, in the TIN123 at 260 °C direct homolysis of the *N*–OR bond has a free energy change of $\Delta G = 123.5$ kJ mol^{-1} and an approximate first order rate coefficient of $k = 8.8$ s^{-1} [33]. At the same temperature, based on previous calculations for similar systems [21], the second-order rate constants for β-hydrogen abstraction from the alkoxyamine range from 10^{-1} to 10^{5} M^{-1} s^{-1} depending on the abstracting radical. Depending on the steady state radical concentrations, it is conceivable that the unimolecular homolysis reaction could be competitive with the bimolecular abstraction reaction at this temperature. In contrast, at 80 °C the homolysis rate coefficient drops to 6.5×10^{-11} s^{-1}, and is uncompetitive with even the slowest abstraction rate coefficients, which in turn range from 10^{-4} to 10^{4} M^{-1} s^{-1}.

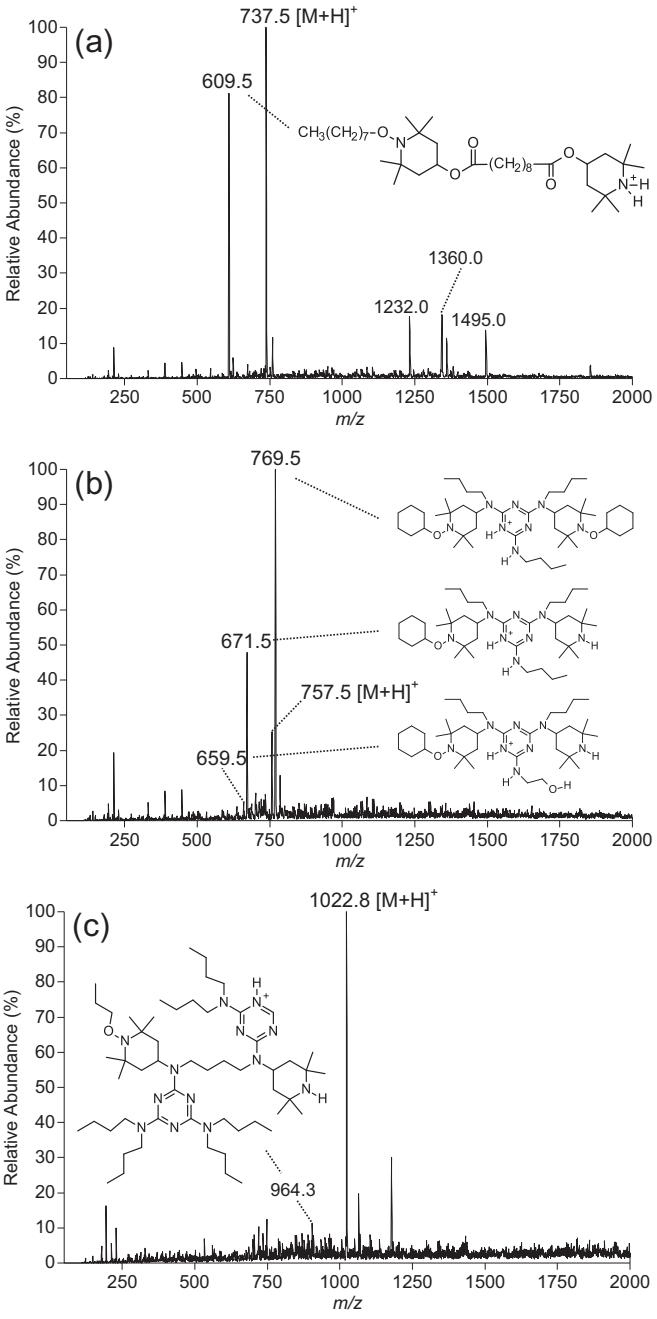

Fig. 5. (a–c) Positive ion DESI-MS spectra of TIN123, TIN152, and TIN NOR371 detected within polyester-based coil coatings after pre-treatment with acetone vapour. Inset – Putative structures for synthetic by-products and *in-situ* structural modifications to precursor HALS compounds present.

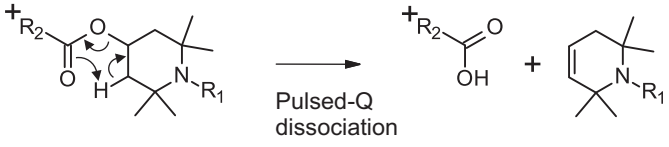

Scheme 3. Fragmentation of ions derived from ester-linked HALS upon pulsed-Q-dissociation inside the mass spectrometer gives rise to characteristic neutral losses depending on the substitution of the piperidine nitrogen. For example, when $R_1 = CH_3$ a neutral loss of 153 Da is observed and where R1 = H a neutral loss of 19 Da is observed (see entries for TIN292 and TIN770, respectively in Table 1).

Table 2
Gas- and solution-phase enthalpies and Gibbs free energies at 260 °C (kJ mol^{-1}) of *N*–OR and *NO*–R homolysis for TIN123, TIN152, and TIN NOR371.[a]

HALS	R	*N*-OR			*NO*-R		
		Gas phase		Solution	Gas phase		Solution
		Δ*H*	Δ*G*	Δ*G*	Δ*H*	Δ*G*	Δ*G*
TIN123	C_3H_7	233.90	118.13	123.49	219.61	109.19	114.77
TIN152	*c*-C_6H_{11}	228.13	113.77	115.00	216.27	101.46	103.02
TIN NOR371	C_3H_7	234.91	118.37	121.73	218.70	106.52	111.52

[a] Electronic energies of homolysis were calculated using double-layer ONIOM approximation to G3(MP2)-RAD method at the R(O)MP2/6-311 + G(3df,2p) level of theory in conjunction with B3LYP/6-31G(d) optimised geometries and scaled frequencies; Free energies of solvation in toluene were calculated using UAKS-PCM/B3LYP/6-31G(d) method. Results at 25 and 80 °C are given in Table S1 of the Supporting Information.

Table 3
Gas- and solution-phase enthalpies and Gibbs free energies at 260 °C (kJ mol^{-1}) of *N*-R homolysis for TIN770, HOST3052, HOST3055, HOST3050, TIN292, TIN144, and HOST3058.[a]

HALS	R	Gas phase		Solution
		Δ*H*	Δ*G*	Δ*G*
TIN770	H	407.48	335.77	362.02
HOST3052	H	406.60	334.31	360.14
HOST3055	H	406.83	334.69	360.90
HOST3050	H	406.58	334.21	360.25
TIN292, TIN144	CH_3	314.50	211.07	233.80
HOST3058	$C(O)CH_3$	326.25	208.16	226.62

[a] Electronic energies of homolysis were calculated using double-layer ONIOM approximation to G3(MP2)-RAD method at the R(O)MP2/6-311 + G(3df,2p) level of theory in conjunction with B3LYP/6-31G(d) optimised geometries and scaled frequencies; Free energies of solvation in toluene were calculated using UAKS-PCM/B3LYP/6-31G(d) method. Results at 25 and 80 °C are given in Table S2 of the Supporting Information.

3.3.6. *N*–CH_3 and *N*–$C(O)CH_3$ HALS

In contrast to alkoxyamines, homolysis of the *N*-R bond is computed to be high in energy for R = H, CH_3 or $C(O)CH_3$ (Table 3). These bond energies are some 150 kJ mol^{-1} greater than those calculated for the alkoxyamine moiety (Table 2) and therefore direct homolysis seems an unlikely pathway to modification at the piperidinyl nitrogen. Indeed, for *N*–CH_3 HALS, activation pathways have been examined previously [21] with the most favoured pathway involving hydrogen abstraction from the *N*–CH_3 group, followed by addition of oxygen, coupling, decomposition to *N*–$CH_2O^{\bullet}$ radical and *β*-scission to the aminyl radical, which then either convert to the secondary amine, or oxidise to the nitroxide (see Scheme 2).

For *N*-deacetylation, several mechanistic routes towards an aminyl radical can be suggested by analogy to the established chemistry of *N*–CH_3 and *N*–OR HALS (Scheme 4). Firstly, abundant reactive polymer radicals R$^{\bullet}$ can attack the carbonyl bond [34] of an initial HALS, adding either to a carbon (Scheme 4, reaction *1*) or an oxygen atom (Scheme 4, reaction *2*). Addition to the carbon side of the carbonyl bond, followed by *β*-scission in the forming *O*-centred radical (Scheme 4, reaction *5*), ultimately leads to an aminyl radical, but is strongly disfavoured on both kinetic and thermodynamic grounds and thus is not likely to be responsible for the experimental observations. Addition to the oxygen side of the carbonyl moiety, likewise, appears to be energetically unfeasible, and, most importantly, does not provide a pathway to an aminyl radical. In contrast, hydrogen abstraction from the *N*–$C(O)CH_3$ group of the initial HALS (Scheme 4, reaction *3*) and subsequent oxidation (Scheme 4, reactions *7-9*) similar to that of the *N*-alkyl HALS adduct (Scheme 2b) [21] represents an energetically feasible route to the aminyl radical. As noted above, *N*–C homolysis (Scheme 4, reaction *4*), on the other hand, does not appear to be competitive with the aforementioned pathway. Once formed, the aminyl radical can abstract a hydrogen atom from, for example, polymer backbone to yield experimentally observed secondary amine or enter one of the regenerative cycles (*cf.* Scheme 1).

4. Conclusion

The detection of ten hindered amine light stabilisers within polyester-based coil coatings by DESI-MS has proven to be rapid, straightforward and able to be performed under ambient conditions. DESI-MS/MS also provides enough qualitative information to enable the characterisation of structural changes occurring to HALS within polyester-based coil coatings. HALS containing a 2,2,6,6-tetramethylpiperidine moiety functionalised at the nitrogen (TIN292, TIN144, HOST3058, TIN123, TIN152, and TIN NOR371) all gave indications of undergoing *in situ* conversion to the corresponding secondary piperidine (*N*–H). These changes occurred under typical curing conditions implying that at least some portion of the initial HALS is actually converted to secondary amine even prior to service. This in turn has implications for their activation and performance under subsequent in-service conditions. Until recently [21] mechanisms for understanding aminoxyl radical regeneration of HALS (such as the Denisov cycle [7–16]) either did not account for a secondary piperidine intermediate or were deemed energetically unfeasible [17,32] yet it is clear from these results that formation of this intermediate constitutes a major pathway in HALS protection of polymers. Recently, two possible

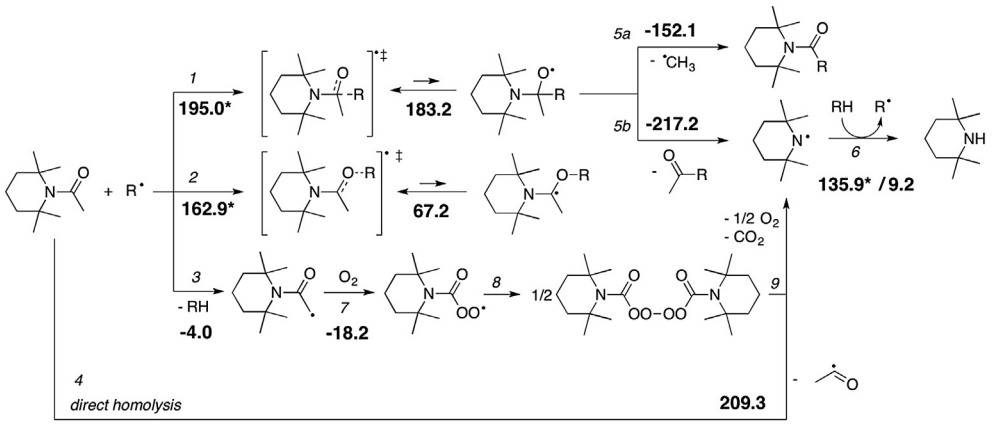

Scheme 4. Formation of aminyl radicals and secondary amines from the thermal decomposition of an *N*-acetyl-piperidine model for the HALS HOST3058: numbers in bold are the Gibbs free energies of reactions (activation*) in gas phase at 260 °C. Results at 25 and 80 °C are given in Table S3 of the Supporting Information.

mechanisms for the formation of the secondary piperidine *in situ* from alkoxyamines have been suggested [21]: (i) by direct *N*-OR bond homolysis or, (ii) *via* hydrogen abstraction and subsequent β-scission. In this work we show that both are consistent with the observed experimental data, though based on high-level quantum chemical calculations, pathway (ii) is dominant under normal service temperatures (25–80 °C), while pathway (i) may become competitive at low radical concentrations and the high temperatures associated with curing (260 °C). Thus both mechanisms warrant strong consideration for all future discussions involving the activation/regeneration of HALS in polymers.

The effectiveness of particular HALS as stabilising agents can be attributed to their ability to remain an active participant in the Denisov cycle, forming and reforming the aminoxyl radical intermediate. Concordantly, resistance to chemical deactivation and/or physical losses including leeching or volatilisation are paramount [35–38]. For these reasons, the stabilising efficacy of different HALS compounds may vary dramatically, being influenced by many factors such as diffusion and solubility coefficients as well as the properties of the coating itself including resin systems, pigment components, curing temperatures and the degree of degradation experienced [12,36,39–41]. In order to optimise HALS compounds, particularly for use in coil coatings, understanding the molecular changes that may occur *in situ* leading to activation or deactivation of HALS and affecting the total active content remaining in the coating after curing is vital.

Acknowledgements

M.R.L.P. and S.J.B. acknowledge funding from the Australian Research Council (ARC) and BlueScope Steel (LP0775032) and S.J.B. and M.L.C. are supported by the ARC Centre of Excellence for Free Radical Chemistry and Biotechnology (CE0561607). G.G. and M.L.C. gratefully acknowledge the generous allocations of computing resources on the National Facility of the Australian National Computational Infrastructure, as well as helpful discussions with Dr Peter Nesvadba. M.R.L.P. is the holder of an Australian Postgraduate Award (Industry).

Appendix A. Supplementary data

Supplementary data related to this article can be found online at http://dx.doi.org/10.1016/j.polymdegradstab.2013.10.026.

References

[1] Gerlock JL, Bauer DR, Briggs LM. Photo-stabilisation and photo-degradation in organic coatings containing a hindered amine light stabiliser. Part I–ESR measurements of nitroxide concentration. Polym Degrad Stab 1986;14:53–71.
[2] Fried JR. Polymer science and technology. 2nd ed. Upper Saddle River, NJ: Prentice Hall PTR; 2003.
[3] Gugumus F. The performance of light stabilizers in accelerated and natural weathering. Polym Degrad Stab 1995;50:101–16.
[4] Pospísil J, Nespurek S. Photostabilization of coatings. Mechanisms and performance. Prog Polym Sci 2000;25:1261–335.
[5] Rabek JF. Photostabilization of polymers: principles and applications. London, UK: Elsevier Applied Science; 1990.
[6] Schaller C, Rogez D, Braig A. Hindered amine light stabilizers in pigmented coatings. J Coat Technol Res 2009;6:81–8.
[7] Bauer DR, Gerlock JL, Mielewski DF. Photodegradation and photostabilization in organic coatings containing a hindered amine light stabilizer. Part VI. ESR measurements of nitroxide kinetics and mechanism of stabilization. Polym Degrad Stab 1990;28:115–29.
[8] Denisov ET. The role and reactions of nitroxyl radicals in hindered piperidine light stabilisation. Polym Degrad Stab 1991;34:325–32.
[9] Eugene NS, Nicholas JT, Peter PK, Matthew EG. Model studies on the mechanism of HALS stabilization. Angew Makromol Chem 1995;232:65–83.
[10] Gugumus F. Mechanisms and kinetics of photostabilization of polyolefins with HALS. Angew Makromol Chem 1990;176:241–89.
[11] Ohkatsu Y. Search for unified action mechanism of hindered amine light stabilizers. J Jpn Pet Inst 2008;51:191–204.
[12] Pospíšil J. Aromatic and heterocyclic amines in polymer stabilization. Springer Berlin/Heidelberg Adv Polym Sci 1995:124–46.
[13] Pospísil J, Pilar J, Nespurek S. Exploitation of the complex chemistry of hindered amine stabilizers in effective plastics stabilization. J Vinyl Addit Technol 2007;13:119–32.
[14] Schwetlick K, Habicher WD. Antioxidant action mechanisms of hindered amine stabilisers. Polym Degrad Stab 2002;78:35–40.
[15] Step EN, Turro NJ, Gande ME, Klemchuk PP. Mechanism of polymer stabilization by hindered amine light stabilizers (HALS)–model investigations of the interaction of peroxy radicals with HALS amines and amino ethers. Macromolecules 1994;27:2529–39.
[16] Xing-Jun H, Scott G. Mechanisms of antioxidant action: the role of O-macroalkyl hydroxylamines in the photoantioxidant mechanism of HALS. Polym Degrad Stab 1996;52:301–4.
[17] Hodgson JL, Coote ML. Clarifying the mechanism of the Denisov cycle: how do hindered amine light stabilizers protect polymer coatings from photooxidative degradation? Macromolecules 2010;43:4573–83.
[18] Paine MRL, Barker PJ, Blanksby SJ. Desorption electrospray ionisation mass spectrometry reveals in situ modification of a hindered amine light stabiliser resulting from direct N-OR bond cleavage. Analyst 2011;136:904–12.
[19] Ananchenko G, Fischer H. Decomposition of model alkoxyamines in simple and polymerizing systems. I. 2,2,6,6-tetramethylpiperidinyl-N-oxyl-based compounds. J Polym Sci Part A Polym Chem 2001;39:3604–21.
[20] Klemchuk PP, Gande ME, Cordola E. Hindered amine mechanisms: part III–investigations using isotopic labelling. Polym Degrad Stab 1990;27:65–74.
[21] Gryn'ova G, Ingold K, Coote ML. New insights into the mechanism of amine/nitroxide cycling during the hindered amine light stabilizer inhibited oxidative degradation of polymers. J Am Chem Soc 2012;134:12979–12.
[22] Schwartz JC. In: Office USP, editor. High-Q pulsed fragmentation in ion traps. U.S.A: ThermoFinnigan; 2005.
[23] Frisch MJ, Trucks GW, Schlegel HB, Scuseria GE, Robb MA, Cheeseman JR, et al. Gaussian 09. Revision A.1 ed. Wallingford CT: Gaussian Inc.; 2009.
[24] Werner H-J, Knowles PJ, Lindh R, Manby FR, Schütz M, Celani P, et al. MOLPRO. 2009.1; 2009.
[25] Izgorodina EI, Yeh Lin C, Coote ML. Energy-directed tree search: an efficient systematic algorithm for finding the lowest energy conformation of molecules. Phys Chem Chem Phys 2007;9:2507–16.
[26] Henry DJ, Sullivan MB, Radom L. G3-RAD and G3X-RAD: modified Gaussian-3 (G3) and Gaussian-3X (G3X) procedures for radical thermochemistry. J Chem Phys 2003;118:4849–60.
[27] Steinfeld JI, Francisco JS, Hase WL. Chemical kinetics and dynamics. Englewood Cliffs, NJ: Prentice Hall; 1989.
[28] Cances E, Mennucci B, Tomasi J. A new integral equation formalism for the polarizable continuum model: theoretical background and applications to isotropic and anisotropic dielectrics. J Chem Phys 1997;107:3032–41.
[29] Lowe TA, Paine MRL, Marshall DL, Hick LA, Boge JA, Barker PJ, Blanksby SJ. Structural identification of hindered amine light stabilisers in coil coatings using electrospray ionisation tandem mass spectrometry. J Mass Spectrom 2010;45:486–95.
[30] DePuy CH, King RW. Pyrolytic cis eliminations. Chem Rev 1960;60:431–57.
[31] Dua S, Bowie JH, Cerda BA, Wesdemiotis C. The facile loss of formic acid from an anion system in which the charged and reacting centres cannot interact. Chem Commun 1998:183–4.
[32] Hodgson JL, Roskop LB, Gordon MS, Lin CY, Coote ML. Side reactions of nitroxide mediated polymerization: N–O versus O–C cleavage of alkoxyamines. J Phys Chem A 2010;38:10458–66.
[33] It should be noted that these rate constants are derived under the assumption that the barrier of activation is defined solely by the reaction free energy, which leads to underestimated values. In reality homolysis would be slightly slower and less competitive.
[34] Henry DJ, Coote ML, Gomez-Balderas R, Radom L. Comparison of the kinetics and thermodynamics for methyl radical addition to C=C, C=O, and C=S double bonds. J Am Chem Soc 2004;126:1732–40.
[35] Cliff N, Kanouni M, Peters C, Yaneff P, Adamsons K. Use of reactable light stabilizers to prevent migration and to improve durability of coatings on plastic substrates. J Coat Technol Res 2005;2:371–87.
[36] Malik J, Ligner G, Ávár L. Polymer bound HALS-expectations and possibilities. Angew Makromol Chem 1997;247:147–61.
[37] Mar'in AP, Borzatta V, Bonora M, Greci L. Diffusion of high molecular weight, sterically hindered amines in polypropylene. J Appl Polym Sci 2000;75:890–6.
[38] Yaneff P, Adamsons K, Cliff N, Kanouni M. Migration of reactable UVAs and HALS in automotive plastic coatings. J Coat Technol Res 2004;1:201–12.
[39] Geuskens G, McFarlane DM. Study of some parameters responsible for the efficiency of hindered amine light stabilizers. J Vinyl Addit Technol 1999;5:186–94.
[40] Malík J, Tuan DQ, Spirk E. Lifetime prediction for HALS-stabilized LDPE and PP. Polym Degrad Stab 1995;47:1–8.
[41] Smoliak LY, Prokopchuk NR. Estimation of parameters that correlate molecular structure of hindered amines with their stabilizing efficiency. Polym Degrad Stab 2003;82:169–72.